Journal of Computational Physics 228 (2009) 8693–8711

Contents lists available at ScienceDirect

Journal of Computational Physics

journal homepage: www.elsevier.com/locate/jcp

# Accuracy preserving limiter for the high-order accurate solution of the Euler equations

Christopher Michalak, Carl Ollivier-Gooch *

*Department of Mechanical Engineering, The University of British Columbia, 2054-6250 Applied Science Lane, Vancouver, BC, Canada V6T 1Z4*

ARTICLE INFO

*Article history:*
Received 5 March 2009
Received in revised form 5 August 2009
Accepted 26 August 2009
Available online 31 August 2009

*Keywords:*
Limiter
High-order accurate
Unstructured mesh
Finite-volume method
Compressible flow

ABSTRACT

Higher-order finite-volume methods have been shown to be more efficient than second-order methods. However, no consensus has been reached on how to eliminate the oscillations caused by solution discontinuities. Essentially non-oscillatory (ENO) schemes provide a solution but are computationally expensive to implement and may not converge well for steady-state problems. This work studies the extension of limiters used for second-order methods to the higher-order case. Requirements for accuracy and efficient convergence are discussed. A new limiting procedure is proposed. Ringleb's flow problem is used to demonstrate that nearly nominal orders of accuracy for schemes up to fourth-order can be achieved in smooth regions using the new limiter. Results for the fourth-order accurate solution of transonic flow demonstrates good convergence properties and significant qualitative improvement of the solution relative the second-order method. The new limiter can also be successfully applied to reduce the dissipation of second-order schemes with minimal sacrifices in convergence properties relative to existing approaches.



## 1. Introduction

High-order discretizations have been shown to reduce computational effort on structured grids [1,2]. High-order finite-volume methods on unstructured grids, although well known [3–5], have not yet effectively been applied to large scale aerodynamics problems. An outstanding issue with these methods is how to deal with discontinuities, such as shocks in the flow, while maintaining good accuracy and convergence.

One means of dealing with discontinuities is to use the classic MUSCL [6] scheme with the addition of a slope limiter. For the second-order case, Barth and Jespersen [7] demonstrated the use of limited reconstruction for the solution of the Euler equations. Efficient convergence to steady state was achieved by Venkatakrishnan [8] by modifying the limiter to be differentiable.

Third-order accurate schemes using *k*-exact reconstruction have been demonstrated first by Barth and Frederickson [3] and subsequently by others [5,9–12, for example]. Transonic and supersonic solutions have been computed in some of these works by various extensions of second-order limiters. However, the work of Barth [9] presents a limiting approach which causes difficulties in steady-state convergence, while other works [5,12] present approaches that do not strictly enforce monotonicity and therefore allow some undesirable oscillations to occur. Furthermore, none of these works formally demonstrate that high-order accuracy is maintained in smooth regions of the flow.

An alternative to MUSCL for obtaining high-order accurate solutions is the essentially non-oscillatory (ENO) scheme [13–15, for instance]. These methods avoid the need for slope limiters by selecting a smooth flux stencil at each iteration. Due to

* Corresponding author. Tel.: +1 604 822 1854; fax: +1 604 822 2403.
*E-mail addresses:* michalak@mech.ubc.ca (C. Michalak), cfog@mech.ubc.ca (C. Ollivier-Gooch).

0021-9991/$ - see front matter © 2009 Elsevier Inc. All rights reserved.
doi:10.1016/j.jcp.2009.08.021

the inherent non-differentiability of this process, convergence of the solution to steady state is not possible. Weighted ENO (WENO) schemes [16–18, for instance] were introduced in part to resolve this issue. However, these schemes do not converge to steady state as efficiently as MUSCL schemes. The computational cost per residual evaluation is also much higher than for reconstruction based solvers. A hybrid between WENO and MUSCL schemes named Quasi-ENO [19] has similar limitations. This method's reconstruction step is much more expensive than traditional MUSCL since the reconstruction least-squares matrix changes at each iteration. For these reasons ENO-like schemes have not seen widespread application to aerodynamics problems.

The present work formulates the requirements and presents a candidate for a limiter that achieves fourth-order accurate solutions in smooth regions while maintaining monotonicity and good convergence properties. Our primary target is monotone shock capturing in steady, transonic flows. Because we limit each primitive variable independently, our approach is in principle applicable to slip lines as well, although in practice most unstructured mesh simulations are poorly resolved along slip lines, rapidly diffusing away this discontinuity. An overview of the high-order MUSCL scheme is given in Section 2. Second-order limiters are reviewed in Section 3. Our extension of these methods to high-order schemes is presented in Section 4. Finally, we present results in Section 5 that demonstrate that our method achieves nominal order of accuracy in smooth regions of the flow while effectively eliminating oscillations at shocks and maintaining good convergence properties.

## 2. High-order accurate solution reconstruction

The third- and fourth-order accurate reconstruction procedure we use here is documented by Ollivier-Gooch and Van Altena [20] and is briefly reviewed in this section. Only the equations that are needed for the discussion of limiters are presented.

In the finite-volume method, the domain is tessellated into non-overlapping control volumes. Each control volume $V_i$ has a geometric reference point $\vec{x}_i$. While in principle any point can be chosen as the reference point, the usual choices (which we recommend) are the cell centroid for cell-centered control volumes and the vertex for vertex-centered control volumes. For any smooth function $U(\vec{x})$ and its control volume averaged values $\overline{U}_i$, the $k$-exact least-squares reconstruction will use a compact stencil in the neighborhood of control volume $i$ to compute an expansion $U_i^R(\vec{x}-\vec{x}_i)$ that conserves the mean in control volume $i$ and reconstructs exactly polynomials of degree $\leqslant k$ (equivalently, $U_i^R(\vec{x}-\vec{x}_i)-U(\vec{x})=\mathcal{O}(\Delta x^{k+1})$).

Conservation of the mean requires that the average of the reconstructed function $U_i^R$ and the original function $U$ over control volume $i$ be the same:

$$\overline{U}_i \equiv \frac{1}{V_i}\int_{V_i} U_i^R(\vec{x}-\vec{x}_i)dA = \frac{1}{V_i}\int_{V_i} U(\vec{x})dA \tag{1}$$

The expansion $U_i^R(\vec{x}-\vec{x}_i)$ can be written as:

$$U_i^R(\vec{x}-\vec{x}_i) = U|_{\vec{x}_i} + \left.\frac{\partial U}{\partial x}\right|_{\vec{x}_i}(x-x_i) + \left.\frac{\partial U}{\partial y}\right|_{\vec{x}_i}(y-y_i) + \left.\frac{\partial^2 U}{\partial x^2}\right|_{\vec{x}_i}\frac{(x-x_i)^2}{2} + \left.\frac{\partial^2 U}{\partial x\partial y}\right|_{\vec{x}_i}((x-x_i)(y-y_i)) + \left.\frac{\partial^2 U}{\partial y^2}\right|_{\vec{x}_i}\frac{(y-y_i)^2}{2} + \cdots \tag{2}$$

Taking the control volume average of this expansion over control volume $i$ and equating it to the mean value gives

$$\overline{U}_i = U|_{\vec{x}_i} + \left.\frac{\partial U}{\partial x}\right|_{\vec{x}_i}\bar{x}_i + \left.\frac{\partial U}{\partial y}\right|_{\vec{x}_i}\bar{y}_i + \left.\frac{\partial^2 U}{\partial x^2}\right|_{\vec{x}_i}\frac{\overline{x^2}}{2} + \left.\frac{\partial^2 U}{\partial x\partial y}\right|_{\vec{x}_i}\overline{xy} + \left.\frac{\partial^2 U}{\partial y^2}\right|_{\vec{x}_i}\frac{\overline{y^2}}{2} + \cdots \tag{3}$$

where

$$\overline{x^n y^m}_i \equiv \frac{1}{A_i}\int_{V_i}(x-x_i)^n(y-y_i)^m dA. \tag{4}$$

are control volume moments. This condition, which must be satisfied exactly, is combined with the reconstruction goal of approximating nearby control volume averages to obtain a constrained least-squares problem for the solution of the Taylor series expansion coefficients. Since the resulting least-squares matrix depends only on geometric terms, its pseudoinverse may be found in a preprocessing step. Therefore the reconstruction step at each flux evaluation is reduced to a matrix–vector product and the exact flux Jacobian can be computed as described in our other work [21]. Ollivier-Gooch [19] presents a modification to the reconstruction procedure resulting in a quasi-ENO scheme. This scheme eliminates the requirement for a limiter by varying the weights of the rows in the least-squares matrix at each iterations based on a measure of smoothness. However, since the pseudoinverse can no longer be precomputed, this scheme is computationally expensive.

## 3. Second-order limiting

To avoid introducing oscillation in the solution process, no new local extrema must be formed during reconstruction. Barth and Jespersen [7] introduced the first limiter for unstructured grids. The scheme consists of finding a limiter value $\Phi_i$ for each primitive flow variable in each control volume that will limit the gradient in the piecewise-linear reconstruction

of the solution. In the second-order reconstruction case, if the reference location $\vec{x}_i$ is taken to be the control volume centroid, the point-wise value $U|_{\vec{x}_i}$ is equal to the control volume average $\overline{U}_i$. This leads to the limited reconstruction of the form

$$U_i^R(\vec{x}-\vec{x}_i,\Phi_i) = \overline{U}_i + \Phi_i \bigtriangledown U_i \cdot (\vec{x}-\vec{x}_i), \quad \Phi \in [0,1]$$

The goal is to find the largest $\Phi_i$ which prevents the formation of local extrema at the flux integration Gauss points. The following procedure is used by Barth and Jespersen:

1. Find the largest negative $\left(\delta U_i^{min} = \min(\overline{U}_j - \overline{U}_i)\right)$ and positive $(\delta U_i^{max} = \max(\overline{U}_j - \overline{U}_i))$ difference between the solution in the immediate neighbors $j$ and the current control volume $i$.
2. Compute the unconstrained reconstructed value at each Gauss point $\left(U_{ik} = U_i^R(\vec{x}_k - \vec{x}_i)\right)$.
3. Compute a maximum allowable value of $\Phi_{ik}$ for each Gauss point $k$.

$$\Phi_{ik} = \begin{cases} \min\left(1, \frac{\delta U_i^{max}}{U_{ik}-\overline{U}_i}\right), & \text{if } U_{ik}-\overline{U}_i > 0 \\ \min\left(1, \frac{\delta U_i^{min}}{U_{ik}-\overline{U}_i}\right), & \text{if } U_{ik}-\overline{U}_i < 0 \\ 1, & \text{if } U_{ik}-\overline{U}_i = 0 \end{cases}$$

4. Select $\Phi_i = \min(\Phi_{ik})$ .
5. Compute the limited reconstruction $U_i^R(\vec{x}-\vec{x}_i,\Phi_i)$ at flux Gauss integration points.

Clearly, steps 1, 3, and 4 introduce non-differentiability in the computation of the reconstructed function. Consequently, the second-order flux is also non-differentiable. This has a severe adverse effect on the convergence properties of the solver. This is particularly evident for implicit schemes, but even explicit time advance schemes are unable to obtain more than two or three orders of magnitude in residual reduction.

In practice, the non-differentiability of step 3 causes the greatest degradation in convergence performance. For this reason, Venkatakrishnan [8] introduces a smooth alternative to step 3 of the Barth–Jespersen procedure by replacing the function $\min(1,y)$ with

$$\phi(y) = \frac{y^2+2y}{y^2+y+2} \tag{5}$$

The effect of this modification can be seen in Fig. 1. This function is differentiable and is entirely contained within the monotonicity bounds derived by Sweby [22] for TVD schemes. Furthermore by satisfying the condition $\phi(2) = 1$ this limiter can be shown to preserve second-order accuracy in regions where no extrema exist for perfectly uniform meshes. Specifically, for smooth solutions on a uniform mesh, the Gauss point is expected to be located at the midpoint connecting two control volume centroids. Therefore for any smooth function $\frac{\delta U_i^{max}}{U_{ik}-\overline{U}_i}$ is expected to be $2 \pm \mathcal{O}(x_i - x_{ik})$, and $\phi(y)$ is therefore expected to be $1 \pm \mathcal{O}(x_i - x_{ik})$. Hence, modifying the gradient in this manner for second-order solutions introduces an error in the reconstruction which is on the order of truncation for smooth flows on uniform grids. However, for general unstructured grids the Gauss point can be located at a distance $\mathcal{O}(x_i - x_{ik})$ away from the midpoint between centroids. Therefore, as will be seen in the results, this limiter leads to accuracy loss relative to the unlimited scheme.

A further modification introduced by Venkatakrishnan is a method to avoid applying the limiter in regions of nearly uniform flow and smooth extrema. In these regions we expect the solution to vary such that $U_{ik} - \overline{U}_i = \mathcal{O}(\Delta x^2)$ where $\Delta x$ is the characteristic length of the control volume $i$. Therefore if the effect of the limiter can be eliminated when $U_{ik} - \overline{U}_i \leqslant (K\Delta x)^{1.5}$,

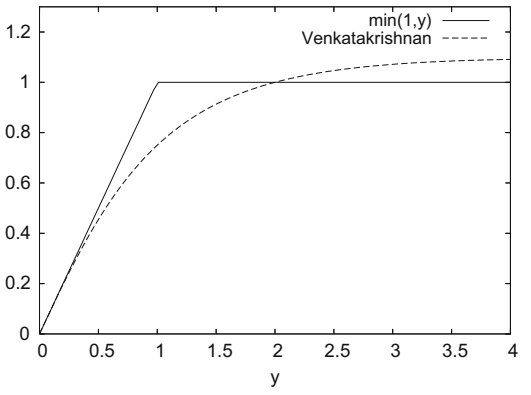


**Fig. 1.** Venkatakrishnan's smooth approximation to $\min(1,y)$.

where $K$ is a tunable parameter, accuracy near smooth extrema can be improved without compromising monotonicity enforcement in other regions.

Venkatakrishnan uses a method inspired by van Albada [23] to make the switch between limited and unlimited regions of flow using a differentiable function so that convergence properties are not adversely affected. For the case $U_{ik} - \overline{U}_i > 0$ the limiter becomes

$$\phi_{ik} = \frac{1}{\Delta_-}\left[\frac{\left(\Delta_+^2 + \epsilon^2\right)\Delta_- + 2\Delta_-^2\Delta_+}{\Delta_+^2 + 2\Delta_-^2 + \Delta_-\Delta_+ + \epsilon^2}\right] \tag{6}$$

In this equation $\Delta_- = U_{ik} - \overline{U}_i, \Delta_+ = \delta U_i^{max}$ and $\epsilon^2 = (K\Delta x)^3$. In addition to improving accuracy this modification is known to be critical to achieving good convergence. When the solution is perturbed in nearly uniform regions or near smooth extrema the results of steps 1 and 4 of the limiting procedure can be expected to change more frequently than in non-uniform regions. Therefore the non-differentiability of these steps is a much greater hindrance to convergence in uniform regions than in non-uniform regions. By effectively disabling the limiter in uniform regions, the addition of the $\epsilon$ term in Eq. (6) greatly improves convergence. The choice of the parameter $K$ is a compromise. Large values of $K$ are favorable to accuracy in smooth regions and good convergence. However, since for any $K > 0$ the limiter no longer strictly enforces monotonicity, large values of $K$ can lead to significant overshoots near discontinuities in the solution.

## 4. High-order limiting

Our high-order limiting scheme follows the same basic outline as traditional second-order limiters. That is, we use Gauss point solution values computed using an unlimited reconstruction to determine whether limiting if necessary. Strictly speaking, this is a necessary but not sufficient condition for monotonicity: higher-order reconstructions admit local extrema within control volumes. One obvious scenario in which the solution would have an extremum within a control volume is the case of a smooth extremum; in this case, we prefer not to limit in order to preserve accuracy, so the fact that our current scheme fails to limit here is an advantage. Near discontinuities, we rely on Gauss point values for practical monotonicity enforcement, on the basis that these are the only values the solver subsequently uses. To improve monotonicity enforcement within control volumes, one could check for monotonicity also at Gauss points for integration over the control volume or even solve the system of equations required to find the extrema of the reconstruction. In the latter case, attention would have to be paid in the implementation to efficiently eliminate cases where the extrema of the reconstruction fall far from the control volume.

### 4.1. Monotonicity

The first challenge of extending the limiting procedure to third- and fourth-order accurate schemes is to express the monotonicity requirement including the high-order reconstruction terms. In second-order schemes the assumption that the solution at the reference point is equal to the control volume average is often made. For cell-centered schemes, where the reference point is the centroid, this assumption is correct. For vertex-centered scheme, the reference point is usually chosen as the vertex location, therefore the assumption is not strictly correct. However, for third- and higher-order schemes the control volume average solution is in general not equal to the centroidal value of the reconstruction. Therefore, when devising a limiter for these schemes, making the distinction between control volume average values and reference-point values becomes critical for maintaining high-order accuracy. With this in mind, the reconstruction polynomial in Eq. (2) can be rewritten in terms of the control volume average with the help of Eq. (3) to yield:

$$\begin{aligned} U_i^R(\vec{x} - \vec{x}_i) = \overline{U}_i &+ \left(\left.\frac{\partial U}{\partial x}\right|_{\vec{x}_i}((x - x_i) - \bar{x}_i) + \left.\frac{\partial U}{\partial y}\right|_{\vec{x}_i}((y - y_i) - \bar{y}_i)\right) \\ &+ \left(\left.\frac{\partial^2 U}{\partial x^2}\right|_{\vec{x}_i}\left(\frac{(x - x_i)^2}{2} - \frac{\overline{x^2}}{2}\right) + \left.\frac{\partial^2 U}{\partial x \partial y}\right|_{\vec{x}_i}((x - x_i)(y - y_i) - \overline{xy}) + \left.\frac{\partial^2 U}{\partial y^2}\right|_{\vec{x}_i}\left(\frac{(y - y_i)^2}{2} - \frac{\overline{y^2}}{2}\right) + \cdots\right) \end{aligned} \tag{7}$$

This can be interpreted as meaning that the reconstructed solution at any point is the control volume average plus second and high-order contributions from the reconstruction:

$$U_i^R(\vec{x} - \vec{x}_i) = \overline{U}_i + S(\vec{x} - \vec{x}_i) + H(\vec{x} - \vec{x}_i)$$

where $H(\vec{x} - \vec{x}_i)$ contains only quadratic terms for third-order reconstruction, and both quadratic and cubic terms for fourth-order reconstruction. Analogous to the second-order case, no new extrema will be formed if

$$\delta U_i^{min} \leqslant S(\vec{x} - \vec{x}_i) + H(\vec{x} - \vec{x}_i) \leqslant \delta U_i^{max}$$

As in the work of Barth [9], the limited form of the high-order accurate reconstruction can be expressed as

$$U_i^R(\vec{x} - \vec{x}_i, \Phi_i) = \overline{U}_i + \Phi_i(S(\vec{x} - \vec{x}_i) + H_i(\vec{x} - \vec{x}_i)) \tag{8}$$

Given this formulation, the same limiting procedure used in Section 3 can be applied to the high-order reconstruction.

Some previous works [5,12] have suggested a formulation where the limiter value multiplies only the second-order terms while the high-order terms are "switched off" when discontinuities are detected. This formulation has the form of

$$U_i^R(\vec{x}-\vec{x}_i,\Phi_i,\sigma_i)=\overline{U}_i+(\Phi_i(1-\sigma_i)+\sigma_i)S(\vec{x}-\vec{x}_i)+\sigma_i H(\vec{x}-\vec{x}_i)$$

where $\sigma_i$, the discontinuity detector, is zero near discontinuities and one in smooth regions of the flow. However, this approach may violate the monotonicity requirement as the high-order terms may have contributed to reducing the overshoot in the unlimited reconstruction used in determining the value of $\Phi_i$. Therefore, the value of $\Phi_i$ computed may be insufficient to reduce the slope such that overshoots occur when the high-order reconstruction terms are disabled. The additional parameters introduced in a smooth switching function for $\sigma_i$ can be considered a further disadvantage.

### 4.2. Accuracy

As previously mentioned, on uniform grids a limiter for the second-order scheme maintains nominal accuracy as long as $|\phi-1|\leqslant\mathcal{O}(\Delta x)$ since this results in an error that is on the order of the quadratic term in the Taylor expansion. However, when a third- or fourth-order scheme is used, the limiter must satisfy $|\phi-1|\leqslant\mathcal{O}(\Delta x^2)$ or $|\phi-1|\leqslant\mathcal{O}(\Delta x^3)$, respectively, for the effect of the limiter in smooth regions to be on the order of truncation error.

For this reason, Venkatakrishnan's limiter will not provide sufficient accuracy even in smooth regions without any local extrema. While the Barth–Jespersen limiter does satisfy these conditions, the lack of differentiability will make achieving a steady-state solution difficult. Therefore, we seek a new approximation for $\min(1,y)$ used in step 3 of the limiting procedure, which we will call $\widetilde{\min}(1,y)$. Like Venkatakrishnan's function, given in Eq. (5), we require that it be differentiable at all points and that it be entirely contained under the function $\min(1,y)$. However, unlike Eq. (5), we also require this new limiting function to have a value of exactly 1 for a range of values $y\geqslant y_t$, where $1<y_t<2$ represents a threshold value. For this function, we propose the form

$$\widetilde{\min}(1,y)=\begin{cases}P(y) & y<y_t\\ 1 & y\geqslant y_t\end{cases}$$

where $P(y)$ is a polynomial satisfying

$$\begin{aligned}&P|_0=0 && P|_{y_t}=1\\ &\left.\frac{dP}{dy}\right|_0=1 && \left.\frac{dP}{dy}\right|_{y_t}=0\\ &P(y)\leqslant\min(1,y), && y\in[0,y_t]\end{aligned}$$

The resulting cubic polynomials for $y_t=1.5,1.75$ are plotted in Fig. 2. This function allows the preservation of high-order accuracy on uniform grids by satisfying $|\widetilde{\min}(1,y)-1|\leqslant\mathcal{O}(\Delta x^3)$. Additionally, this function is also effective in maintaining high-order accuracy in regions of mild mesh non-uniformity. The degree of non-uniformity that can be accommodated is dictated by the choice of the threshold value $y_t$. Smaller values of $y_t$ are less likely to unduly activate the limiter on non-uniform meshes but result in a limiter that approaches non-differentiability. Therefore the choice of $y_t$ is a compromise between maintaining good accuracy on non-uniform grids and maintaining good convergence properties. For the results presented in this work, we use $y_t=1.5$ which yields the following cubic polynomial

$$P(y)=-\frac{4}{27}y^3+y$$

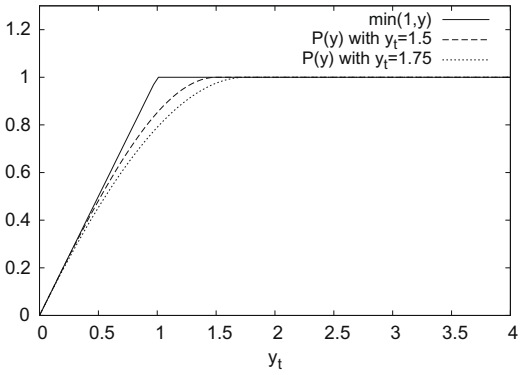


**Fig. 2.** $\widetilde{\min}(1,y)$ with $y_t=1.5$ and $y_t=1.75$ compared to $\min(1,y)$.

### 4.3. Uniform regions and smooth extrema

For the reasons already mentioned in Section 3, it is desirable to eliminate the effect of the limiter in regions of uniform flow or near smooth extrema. To maintain high-order accuracy it is essential to permit monotonicity to be violated near smooth extrema. Furthermore the limiter value changes rapidly and is non-differentiable in uniform regions which prevents good convergence of the solver. Therefore, analogous to the second-order limiter of Venkatakrishnan, we wish to eliminate the effect of the limiter when the local solution variation is $\mathcal{O}(\Delta x^2)$ or smaller. Specifically, we propose to disable the limiter when

$$\delta U \equiv (\delta U_i^{max} - \delta U_i^{min}) < (K\Delta x)^{\frac{3}{2}}$$

where $K$ is a tunable parameter. However, using a simple switch would introduce a non-differentiable step in the residual evaluation which would cause convergence problems. Therefore, to maintain differentiability, the following procedure is proposed:

$$\widetilde{\Phi}_i = \widetilde{\sigma}_i + (1 - \widetilde{\sigma}_i)\Phi_i \tag{9}$$

where $\Phi_i$ is the limiter value as calculated in step 4 of the procedure in Section 3 and $\tilde{\sigma}_i$ is the following function:

$$\tilde{\sigma}_i = \begin{cases} 1 & \delta U^2 \leqslant (K\Delta x)^3 \\ s\left(\frac{\delta U^2 - (K\Delta x)^3}{(K\Delta x)^3}\right) & (K\Delta x)^3 < \delta U^2 < 2(K\Delta x)^3 \\ 0 & \delta U^2 \geqslant 2(K\Delta x)^3 \end{cases} \tag{10}$$

where the transition function $s$ is defined by

$$s(y) = 2y^3 - 3y^2 + 1 \tag{11}$$

and is plotted in Fig. 3. The limited reconstruction is then computed for each Gauss point by evaluating $U_i^R(\vec{x} - \vec{x}_i, \widetilde{\Phi}_i)$.

Although this two stage limiting procedure is somewhat more computationally expensive than Venkatakrishnan's limiter in the general case, some "short circuiting" is possible in uniform regions of flow. Since $\tilde{\sigma}_i$ depends only on neighboring control volume averages, unlike $\Phi_i$ which also depends on an evaluation of the unconstrained reconstruction at each Gauss point, it is relatively inexpensive to compute. When $\tilde{\sigma}_i$ evaluates to 1, computational effort can be saved by not computing $\Phi_i$ since it does not affect the value of the final limiter $\widetilde{\Phi}_i$.

We emphasize that, although the threshold below which we consider the solution to be flat—and therefore choose not to limit—has the same form as the parameter in Venkatakrishnan's limiter that addresses the same issue, the two approaches differ significantly in their action. Venkatakrishnan's $\epsilon^2$ term modifies the limiter value for all cases, and increasing the value of $K$ allows a progressively larger overshoot in the solution at shocks. In our case, near shocks the transition function is exactly one, and the basic limiter enforces monotonicity regardless of the value of $K$. As we will show in Section 5.2.4, our scheme is less sensitive than Venkatakrishnan's to the choice of $K$.

### 4.4. Boundary treatment

Maintaining high-order accuracy near domain boundaries represents a special challenge. Local extrema are expected to exist on the boundary for smooth flows. Unlike smooth extrema in the interior of the domain, these points are not

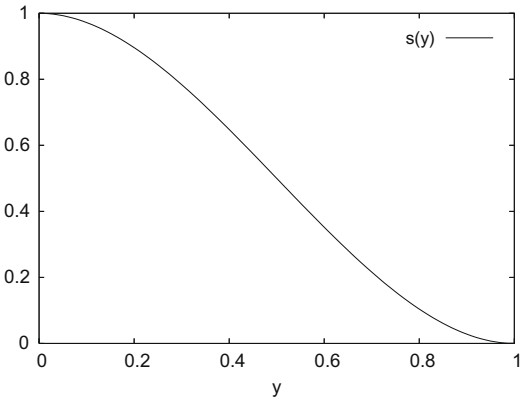


**Fig. 3.** Transition function $s(y) = 2y^3 - 3y^2 + 1$ used to smoothly disable the limiter in nearly uniform regions.

characterized by a zero first derivative of flow property with respect to space. Therefore, the method used in Section 4.3 will not be effective in disabling the limiter in these regions.

As a first measure, in our implementation of both Venkatakrishnan and the new limiter we elect to only iterate over interior face Gauss points in step 3 of the limiting procedure. Therefore an extremum forming on a boundary Gauss point will not cause the limiter to activate. In our experience this does not cause any oscillatory issues at shocks. However, the Gauss points on interior faces of boundary control volumes will often also have reconstructed values of smooth solutions that form an extremum relative to the control volume averages of the solution in the reconstruction stencil. In some cases even Gauss points of control volumes adjacent to boundary control volumes will exhibit this behavior. In our experience eliminating all of these Gauss points from step 3 of the limiting procedure causes unacceptable oscillations in the solution near shocks. Therefore, to maintain high-order accuracy near boundaries while maintaining solution monotonicity another approach is needed.

Thus far the proposed limiting procedure is entirely physics agnostic. However, we have been unable to find a satisfactory means of dealing with the issue of accuracy and monotonicity of boundary and near-boundary control volumes in this manner. Therefore we propose a method specific to the Euler equations.

For external and many internal flows the far-field boundary usually has nearly uniform flow conditions. For these boundaries the limiter is effectively disabled by the method applied in Section 4.3. Therefore we will focus our attention on the wall boundary. Two flow conditions can be present at a wall boundary condition: the flow can be tangential to the wall, or it can be a stagnation point. We propose methods for maintaining high-order accuracy in both cases.

#### 4.4.1. Tangential flow

For every wall boundary control volume we will consider a "ghost" control volume which is a mirror image of the boundary control volume about the boundary. It will have an approximate control volume average value of the solution assigned to it consistent with a shockless flow. These values will be used to expand the stencil used to determine monotonicity outside of the flow domain. This will effectively make the near-boundary reconstructed Gauss point values no longer extrema for smooth flows. To preserve high-order accuracy, these ghost control volume values will not be used in the least-squares reconstruction process. They will only be used when determining the values of $\delta U_{min}$ and $\delta U_{max}$ in the limiting procedure. For any control volume that includes the boundary control volume as its first neighbor the respective mirror control volume will also be included in determining $\delta U_{min}$ and $\delta U_{max}$.

To determine an appropriate solution value for the mirror control volume we begin by noting that any well resolved curved boundary locally resembles a circular arc. We approximate the radius of curvature from the boundary Gauss point normals of the curved boundary edges. Since this information is needed by the high-order boundary flux integration scheme, it is readily available. Next, we apply the steady momentum equation in the direction normal to the streamline

$$\frac{\partial P}{\partial n} = -\frac{\rho V^2}{R}$$

where $n$ is the direction normal to the wall, $\rho$ is density, $V$ is velocity and $R$ the radius of curvature. Since the ghost value is only used in computing the limiter, a first-order approximation is sufficient. We can therefore approximate the ghost value of pressure by

$$\overline{P}_{gi} = \overline{P}_i - 2d \cdot \frac{\bar{\rho}_i \overline{V}_i^2}{R} \tag{12}$$

where $\overline{P}_i$, $\bar{\rho}_i$, and $\overline{V}_i$ are the control volume pressure, density and velocity, respectively, and $d$ is the distance of the control volume centroid from the wall in the convex direction ($d$ is negative for concave boundaries). The ghost values of Mach number and density can be obtained by considering the isentropic transformation from the control volume state to the ghost value state with a pressure of $\overline{P}_{gi}$

$$\bar{\rho}_{gi} = \bar{\rho}_i \left( \frac{\overline{P}_{gi}}{\overline{P}_i} \right)^{\frac{1}{\gamma}}$$

$$\overline{M}_{gi}^2 = \frac{2}{\gamma - 1} \left( \left( \frac{\overline{P}_{t_i}}{\overline{P}_{gi}} \right)^{\frac{\gamma-1}{\gamma}} - 1 \right)$$

where $\overline{M}_{gi}$ is the Mach number in the ghost control volume and $\overline{P}_{t_i}$ is the total pressure as calculated using the boundary control volume average flow properties. This, together with the assumption that the flow direction remains tangential to the surface, fully establishes the state of the ghost control volume.

#### 4.4.2. Stagnation point

Additional steps need to be taken to prevent the application of the limiter at stagnation points. Although affecting a very small fraction of control volumes, obtaining high-order accuracy near stagnation points can be critical to global accuracy.

In practical aerodynamics problems, the flow discontinuity which requires the proper application of the limiter is the shock. Since supersonic flow is required to produce a shock, and stagnation points are necessarily in subsonic regions, it is possible to simply disable the limiter in the latter areas. Specifically, we propose that the reconstruction of a control volume can only be adversely affected by a shock if at least one of the control volumes in its reconstruction stencil contains supersonic flow. Practically, we wish to smoothly disable the limiter as the highest control volume average Mach number in the reconstruction stencil is reduced. For this purpose we can reuse the approach of Section 4.3. Specifically, the limiter value is once again modified such that

$$\widehat{\Phi}_i = \hat{\sigma}_i + (1 - \hat{\sigma}_i)\widetilde{\Phi}_i, \tag{13}$$

where $\widetilde{\Phi}_i$ is the limiter value after applying the uniform-flow fix in Eq. (9) and

$$\hat{\sigma}_i = \begin{cases} 1 & M_{i,max} \leqslant M_1 \\ s\left(\frac{M_{i,max}-M_1}{M_2-M_1}\right) & M_1 < M_{i,max} < M_2 \\ 0 & M_{i,max} \geqslant M_2 \end{cases} \tag{14}$$

where $M_{i,max}$ is the maximum Mach number of the control volume averages of the reconstruction stencil of control volume $i$, and $s$ is the function in Eq. (11). The parameters $M_1$ and $M_2$ define the Mach numbers at which the effect of the limiter is fully disabled and fully enabled, respectively. In the present work we use $M_1 = 0.8$ and $M_2 = 0.85$; lower values would be beneficial for sharper resolution of a slip line in transonic flow. The new limited reconstruction used by the flux integration scheme becomes $U_i^R(\vec{x} - \vec{x}_i, \widehat{\Phi}_i)$. For typical aerodynamic flows there is no harm in applying this step to all control volumes, even if they are not near boundaries. Doing so can reduce computational effort since $\widetilde{\Phi}_i$ does not need to be evaluated if $\hat{\sigma}_i$ evaluates to 1.

### 4.5. Complete algorithm

The complete algorithm is, in the general case, more complex and costly than the second-order limiting procedure presented in Section 3. However, the various additions can, in some cases, be used to "short circuit" the evaluation of the limiter, therefore reducing computational effort. The complete algorithm for applying the limiter to the reconstruction for each flow property of each control volume is

1. Find the maximum Mach number of the reconstruction neighbors control volume averages of the solution and evaluate $\hat{\sigma}_i$ using Eq. (14). If $\hat{\sigma}_i = 1$ then $\widehat{\Phi}_i = 1$ and the algorithm jumps to step 9.
2. Find the largest negative $\left(\delta U_i^{min} = \min(\overline{U}_j - \overline{U}_i)\right)$ and positive $(\delta U_i^{max} = \max(\overline{U}_j - \overline{U}_j))$ difference between the solution in the immediate neighbors $j$ and the current control volume $i$. If the control volume or any of its immediate neighbors are adjacent to a wall boundary include their ghost values using Eq. (12) and isentropic relations.
3. Compute $\tilde{\sigma}_i$ using Eq. (10). If $\tilde{\sigma}_i = 1$ then $\widehat{\Phi}_i = \widetilde{\Phi}_i = 1$ and the algorithm jumps to step 9.
4. Compute the unconstrained reconstructed value at each Gauss point $\left(U_{ik} = U_i^R(\vec{x}_k - \vec{x}_i)\right)$.

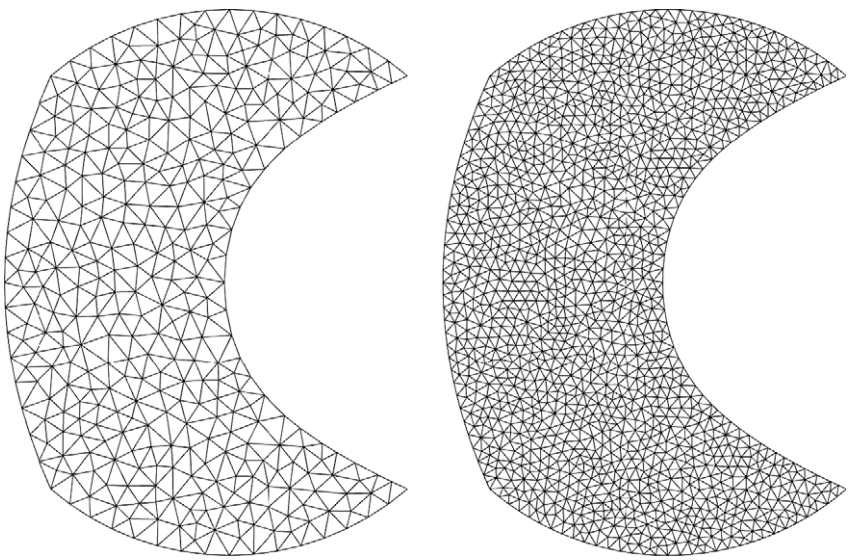

**Fig. 4.** Two coarsest meshes used for Ringleb's flow test case.

5. Compute a maximum allowable value of $\phi_{ik}$ for each Gauss point $k$.

$$\phi_{ik} = \begin{cases} \widetilde{\min}\left(1, \frac{\delta U_i^{max}}{U_{ik} - \overline{U}_i}\right), & \text{if } U_{ik} - \overline{U}_i > 0 \\ \widetilde{\min}\left(1, \frac{\delta U_i^{min}}{U_{ik} - \overline{U}_i}\right), & \text{if } U_{ik} - \overline{U}_i < 0 \\ 1, & \text{if } U_{ik} - \overline{U}_i = 0 \end{cases}$$

6. Select $\Phi_i = \min(\phi_{ik})$ .
7. Compute $\widetilde{\Phi}_i$ using Eq. (9).
8. Compute $\widehat{\Phi}_i$ using Eq. (13).
9. Compute the limited reconstruction $U_i^R(\vec{x} - \vec{x}_i, \widehat{\Phi}_i)$ at flux Gauss integration points using Eq. (8).

## 5. Results

The presented results were obtained using a Newton-GMRES [24] vertex-centered finite-volume solver. The solution process consists of two stages. In the preiteration stage the linear system resulting from a local timestepping is solved at each

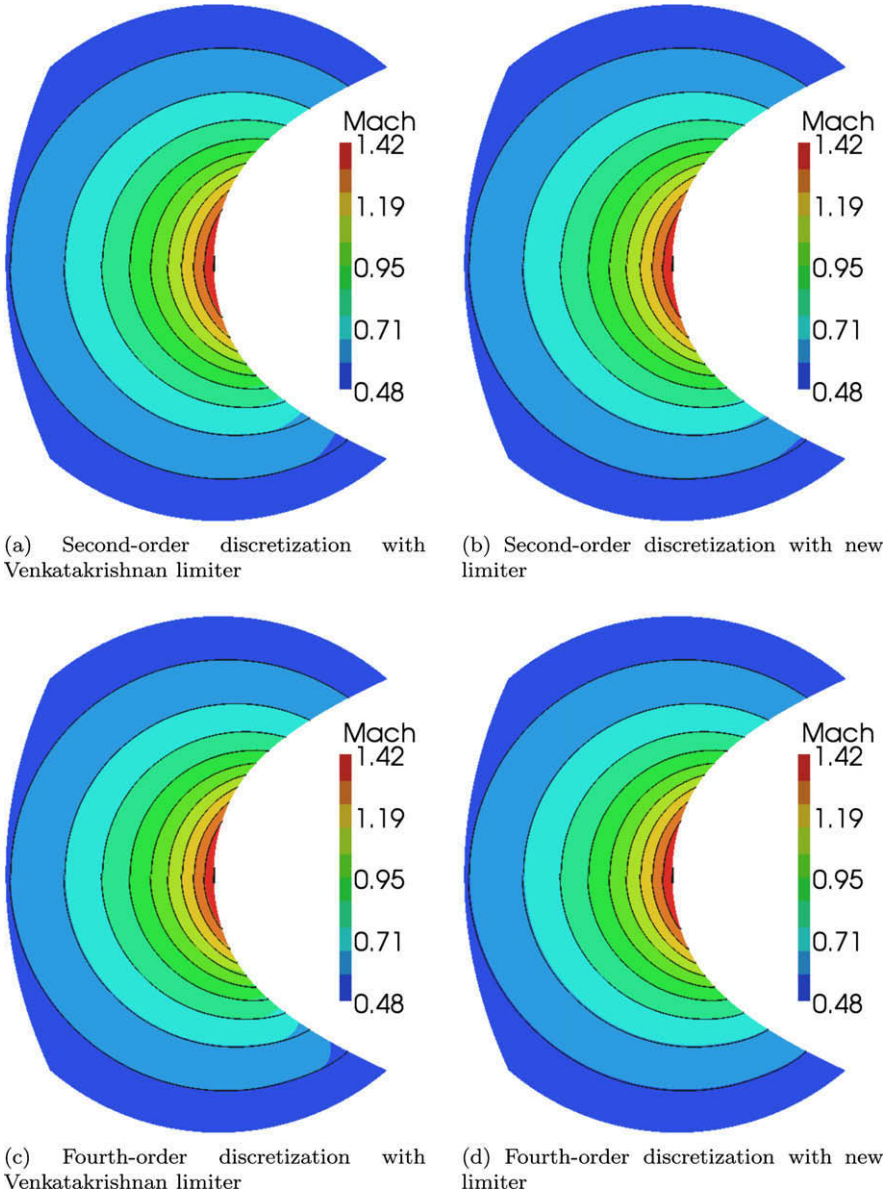


(a) Second-order discretization with Venkatakrishnan limiter

(b) Second-order discretization with new limiter

(c) Fourth-order discretization with Venkatakrishnan limiter

(d) Fourth-order discretization with new limiter

**Fig. 5.** Mach number contours from numerical solution of Ringleb's flow on 1426 control volume mesh. Each subfigure also shows line contours of Mach number for the fourth-order discretization with the new limiter for comparison.

iteration. The Jacobian from the first-order accurate scheme is used on the left-hand side and the full-order accurate flux is used on the right-hand side. At each Newton iteration, the linear system is approximately solved using incomplete-lower-upper factorization (ILU) preconditioned GMRES. During the second stage, the left-hand side is replaced with the full-order accurate Jacobian [21].

In addition to results using the new limiter, results are also presented for the high-order scheme using the procedure in Section 4.1 but with Venkatakrishnan's limiting function. For Venkatakrishnan's function we use a tuning parameter of $K = 2$ and for the new limiter we use $K = 1$.

### 5.1. Ringleb's flow

We begin by considering Ringleb's flow which is transonic but shockless and has a known exact solution. This will enable us to quantify the negative effects of Venkatakrishnan's limiter and the new limiter on the accuracy of the solution in smooth regions of flow. We consider four meshes consisting of 369, 1426, 5467 and 20,690 control volumes. The two coarsest meshes are shown in Fig. 4.

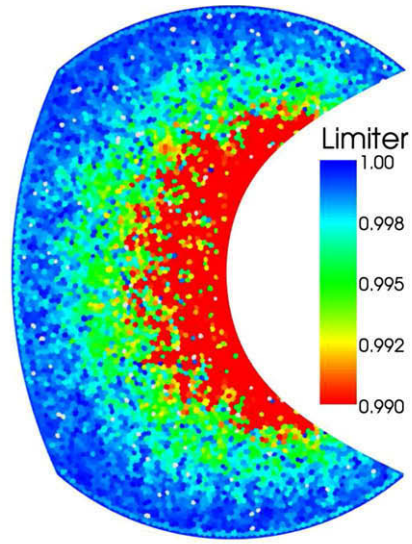


(a) Venkatakrishnan's limiter

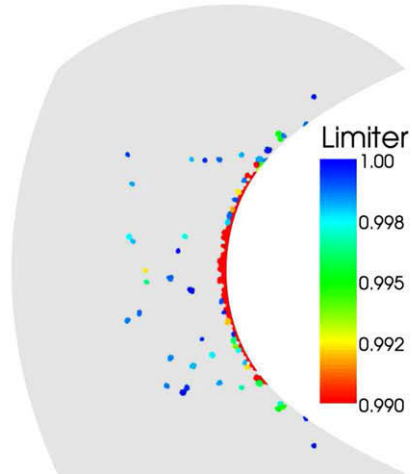


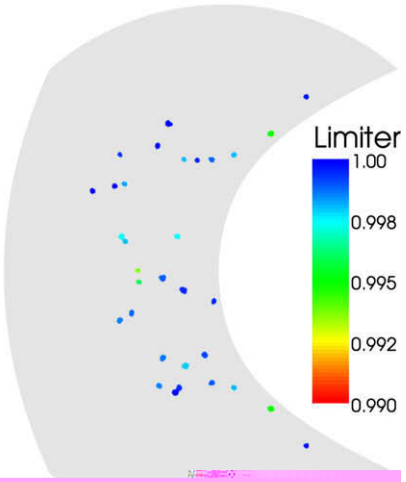


New limiter without boundary ghost cells (c) New limiter (b) valu

**Fig. 6.** Limiter value for pressure for the fourth-order converged solution on the 5467 control volume mesh. Only values $\Phi \neq 1$ are plotted.

The exact solution to Ringleb's flow is given by the streamlines defined by:

$$x = \frac{1}{2}\frac{1}{\rho}\left(\frac{1}{q^2} - \frac{2}{k^2}\right) + \frac{J}{2}$$
$$y = \pm\frac{1}{k\rho q}\sqrt{1 - \left(\frac{q}{k}\right)^2}$$

where $k$ is constant along streamlines and

$$q = |\vec{V}|$$
$$J = \frac{1}{c} + \frac{1}{3c^3} + \frac{1}{5c^5} - \frac{1}{2}\ln\frac{1+c}{1-c}$$
$$c = \sqrt{1 - \frac{\gamma - 1}{2}q^2}$$
$$\rho = c^{2/(\gamma-1)}$$

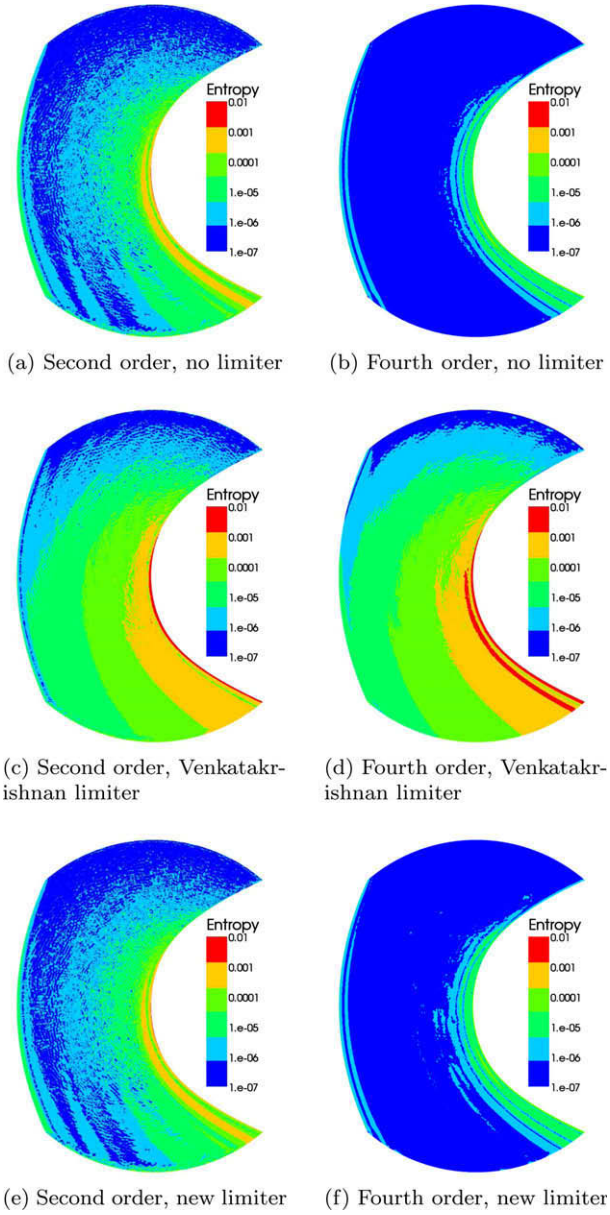


(a) Second order, no limiter (b) Fourth order, no limiter

(c) Second order, Venkatakrishnan limiter (d) Fourth order, Venkatakrishnan limiter

(e) Second order, new limiter (f) Fourth order, new limiter

**Fig. 7.** Difference in dimensionless entropy from the freestream value for Ringleb's flow.

The computational domain is constructed using solid walls at the streamlines for $k = 0.55, 1.2$ and placing the inlet and outlet at $q = 0.5$. This results in a geometry that is symmetric about the horizontal axis. The flow is subsonic at the inlet and outlet but is supersonic near the inside wall of the throat. Using this domain, rather than just the upper half, is a more stringent test of the accuracy of the computational scheme since errors produced at the throat are allowed to propagate to the lower half of the domain.

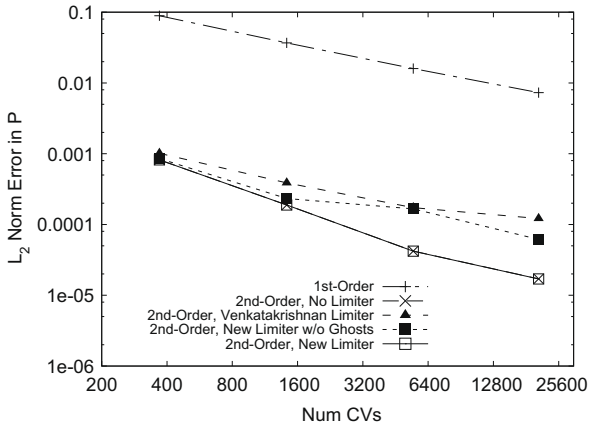


**(a) Second-order discretization**

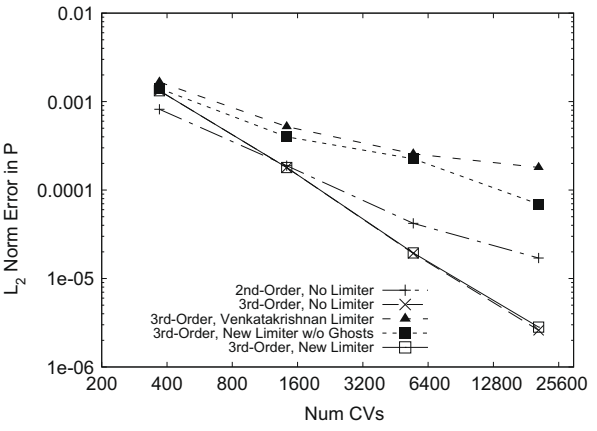


**(b) Third-order discretization**

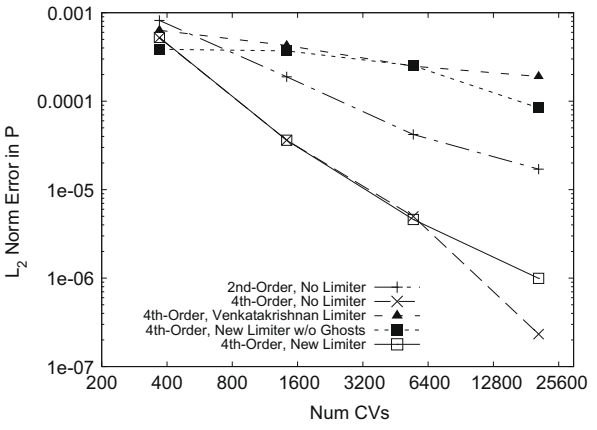


**(c) Fourth-order discretization**

**Fig. 8.** Error convergence for pressure in Ringleb's flow.

Since this test case contains no stagnation points, the Mach number dependent deactivation of the limiter should not be necessary. For this reason, and to make the test as stringent as possible, we do not apply steps 1 and 8 of the high-order limiting procedure as presented in Section 4.5.

As an initial qualitative assessment, we compare the Mach number contours generated on the 1426 control volume mesh using Venkatakrishnan's limiter and the new limiter in Fig. 5. Each subfigure shows the Mach number distribution for the scheme identified in its caption, with line contours for the new limiter with the fourth-order scheme added to highlight differences between schemes. The additional dissipation of the Venkatakrishnan limited solutions is evident in the reduced Mach number at the inner wall near the outflow. Using the same criterion we can visually detect a slight superiority of the fourth-order scheme over the second-order scheme when using the new limiter. The Venkatakrishnan limited procedure, on the other hand, does not benefit from the use of the high-order accurate reconstruction.

Next we examine the value of the limiter value $\Phi$ for the pressure component at steady state for the fourth-order solution on the 5467 control volume mesh using the two limiting schemes in Fig. 6. In addition to Venkatakrishnan's limiter and the new limiter, we also consider the new limiter without the special boundary ghost value treatment introduced in steps 3 and 7 of the high-order limiting procedure. The new limiter successfully avoids limiting in almost all control volumes; the fraction of control volumes where the limiter is active remains about the same with mesh refinement. All the control volumes that are limited have values $\Phi \geqslant 0.99$, although this bound becomes somewhat lower with mesh refinement. Without the boundary ghost treatment significant limiting occurs near the inner wall boundary. Venkatakrishnan's limiter, on the other hand, applies some limiting to virtually all control volumes.

Next, in Fig. 7, entropy is plotted for the second- and fourth-order schemes on the second-finest grid. The new limiter causes no distinguishable additional entropy production relative to the unlimited scheme for the second-order method, and a very slight increase for the fourth-order method. On the other hand, Venkatakrishnan's limiter increases entropy by

**Table 1**
Convergence order of norms of error in pressure for Ringleb's flow computed using regression fit of all mesh results.

| Nominal order | Limiter | $L_1$ norm | $L_2$ norm | $L_\infty$ norm |
|---|---|---|---|---|
| 1st | None | 1.24 | 1.24 | 0.99 |
| 2nd | None | 2.22 | 1.96 | 1.24 |
| 2nd | Venkatakrishnan | 1.10 | 1.07 | 0.47 |
| 2nd | New w/o Ghosts | 1.71 | 1.23 | 0.47 |
| 2nd | New | 2.22 | 1.96 | 1.24 |
| 3rd | None | 3.18 | 3.12 | 2.70 |
| 3rd | Venkatakrishnan | 1.14 | 1.10 | 0.51 |
| 3rd | New w/o Ghosts | 1.83 | 1.43 | 0.59 |
| 3rd | New | 3.14 | 3.08 | 2.40 |
| 4th | None | 4.07 | 3.74 | 3.06 |
| 4th | Venkatakrishnan | 0.62 | 0.62 | 0.12 |
| 4th | New w/o Ghosts | 1.07 | 0.74 | 0.23 |
| 4th | New | 3.24 | 3.11 | 2.08 |

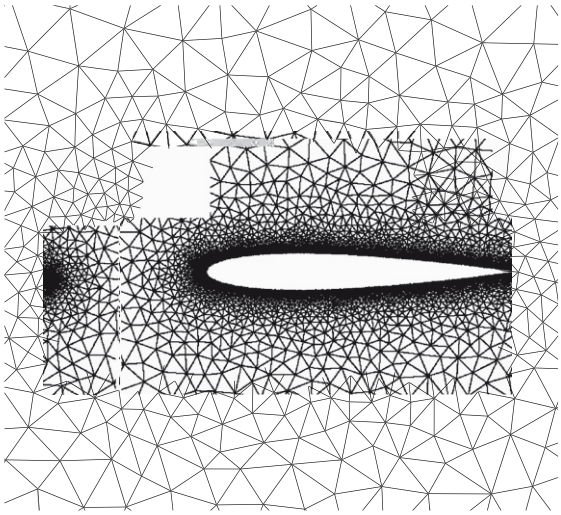

**Fig. 9.** Mesh consisting of 4656 control volumes used for the NACA 0012 test case.

approximately an order of magnitude for the second-order scheme and two to four orders for the fourth-order scheme. Once again we note that when applying Venkatakrishnan's limiter there is no apparent benefit to using the fourth-order scheme over the second-order scheme.

The $L_2$ norm of error of the converged solution compared to the known exact solution is used to generate Fig. 8. The grid-convergence orders of the error norms using a regression fit of the results from all grids are given in Table 1. We begin by noting that the unlimited schemes attain their nominal orders of accuracy in $L_1$ and $L_2$ norms and one order accuracy less than nominal for the $L_\infty$ norm. Although the error of second-, third-, and fourth-order schemes using Venkatakrishnan's limiter is lower than that of the first-order scheme, the error does not converge with nominal accuracy. In fact the grid convergence of the error when using Venkatakrishnan's limiter is only first-order. The results using the new limiter without the boundary ghost value treatment outperform Venkatakrishnan's limiter only slightly. This indicates that the application of the limiter in even an isolated region has severe implications for global accuracy. The new limiter with boundary ghost values, on the other hand, allows for the second- and third-order schemes to perform virtually identically to the unlimited case and has an adverse effect on the accuracy of the fourth-order scheme only on the finest mesh. The problem here is that, on realistic unstructured meshes, mesh irregularities can induce limiter activity in smooth regions of the flow. To leading order, this alters the reconstructed solution values used in flux integration by $O(|\nabla u|(1-\phi)h)$, where $\nabla u$ is the gradient of the solution and $h$ is the characteristic size of the control volume. For coarse meshes and lower orders of accuracy, the impact of

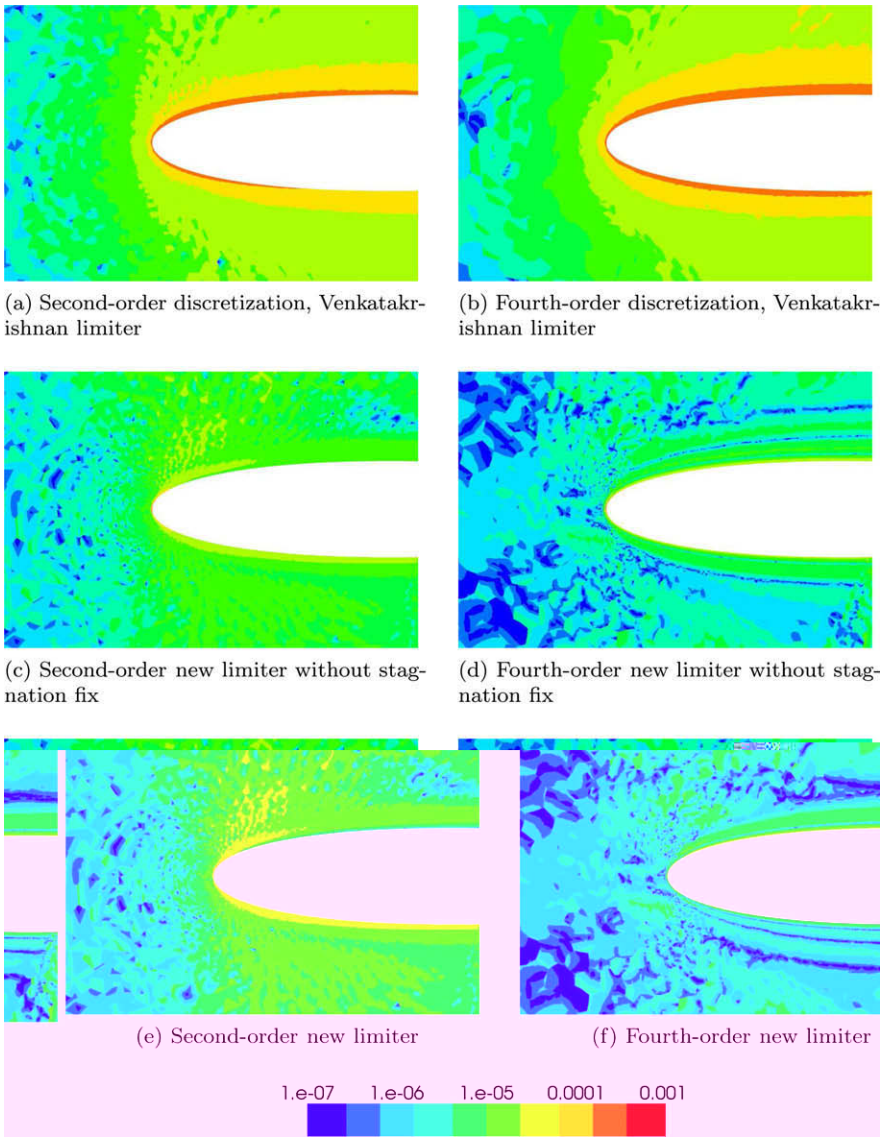


**Fig. 10.** Difference in dimensionless entropy from the freestream value for Mach 0.8, $\alpha = 1.25^\circ$ flow around a NACA 0012 airfoil.

these inadvertent limiter firings is lost in the larger discretization error. However, for fourth-order and fine meshes, the discretization error is low enough that this effect comes to dominate the error. While clearly undesirable, this limiter error is still quite small compared with the analogous error introduced by Venkatakrishnan's limiter.

### 5.2. Transonic flow over an airfoil

Next, we present results for transonic flow over a NACA 0012 airfoil at Mach 0.8 and an angle of attack of 1.25°. The computational mesh consists of 4656 control volumes and is shown in Fig. 9. We will consider second- and fourth-order schemes using Venkatakrishnan's limiter, the new limiter, and the new limiter without the stagnation region fix which disables the limiter at low Mach number in steps 1 and 8 of the high-order limiting procedure.

#### 5.2.1. Accuracy

We begin by assessing the quality of the solution upstream of the shock. Entropy near the leading edge of the airfoil is plotted in Fig. 10. The fourth-order solution with Venkatakrishnan's limiter once again fails to outperform its second-order counterpart. The new limiter produces approximately an order of magnitude less entropy than Venkatakrishnan's limiter for the second-order scheme. The new limiter applied to the fourth-order scheme results in even less entropy production. Disabling the stagnation region fix results in a modest increase in entropy production.

The quality of the solutions can also be compared by examining the stagnation pressure ratio along the upper surface of the airfoil shown in Fig. 11. The decrease in total pressure across the shock is comparable for all schemes. However, the schemes limited with the Venkatakrishnan limiter result in substantial stagnation pressure loss upstream of the shock. For the second-order scheme the stagnation region fix has little effect while for the fourth-order scheme applying this step in the limiting procedure results in a further improvement in the conservation of total pressure.

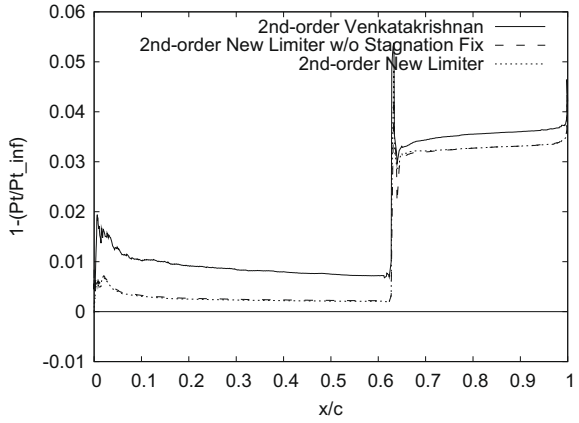


**(a) Second order**

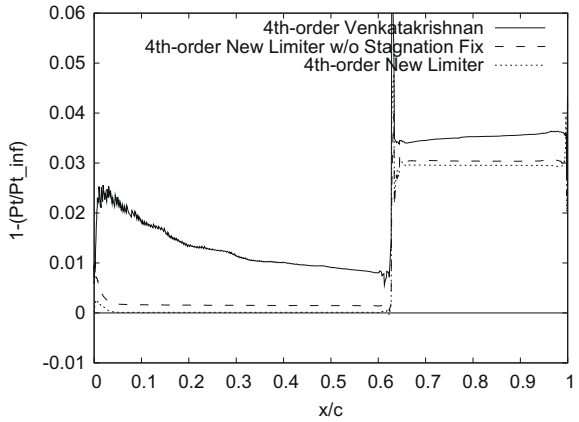


**(b) Fourth order**

**Fig. 11.** Decrease in total pressure along the upper surface of the NACA 0012 airfoil at Mach 0.8 $\alpha = 1.25$.

*5.2.2. Shock monotonicity*

The performance of the new limiter in controlling oscillations and overshoots in the solution near the strong shock on the upper surface of the airfoil is demonstrated in the pressure plot of Fig. 12. The new limiter and Venkatakrishnan's limiter are both effective in eliminating any substantial oscillations near the shock. The pressure computed on the upper surface of the airfoil using the different limiters is virtually indistinguishable. Once again the lower dissipation of the new limiter is demonstrated by the sharper profile of the weak shock on the lower surface of the airfoil.

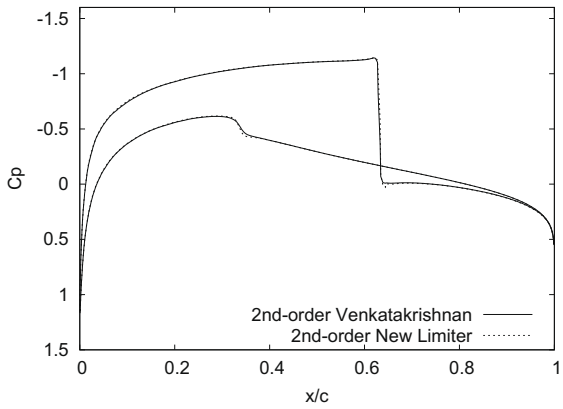


**(a) Second order**

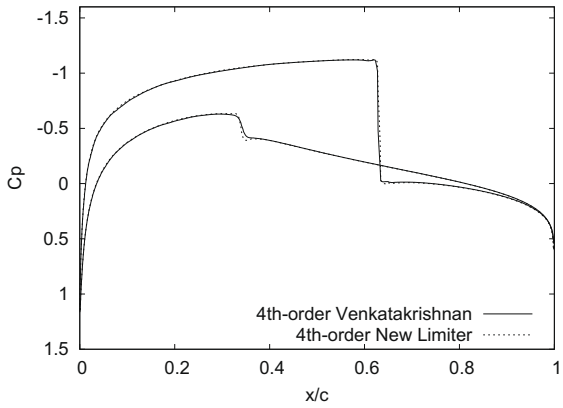


**(b) Fourth order**

**Fig. 12.** Surface pressure profiles for transonic flow over a NACA0012 airfoil.

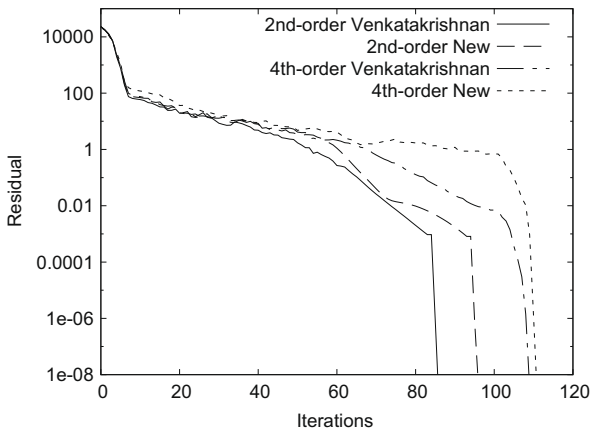


**Fig. 13.** Convergence history for transonic airfoil case.

*5.2.3. Convergence*

Next, we consider the residual convergence properties of the new limiting scheme coupled with our Newton-GMRES solver. Fig. 13 shows the convergence of the scheme with the new limiter relative to Venkatakrishnan's limiter for second and fourth-order accurate schemes. We have also provided the computational time required for convergence in Table 2.

The scheme with the new limiter exhibits a slightly poorer convergence rate than Venkatakrishnan's limiter. This is likely due to the lower dissipation of the scheme which results in poorer conditioning of the nonlinear system of equations. Similarly, we find that the fourth-order scheme requires slightly more iterations to converge than the second-order scheme.

*5.2.4. Sensitivity to tuning parameter*

Venkatakrishnan's limiter and the new limiter both require a tuning parameter $K$ to detect regions of uniform flow. Ideally the solutions produced by the schemes should be relatively insensitive to the choice of this parameter. Therefore we consider the effect of increasing and decreasing the parameter by a factor of 4 from the original choice. For Venkatakrishnan's scheme we consider $K = 0.5, 2, 8$ and for the new limiter we consider $K = 0.25, 1, 4$. In Fig. 14 we examine the behavior of

**Table 2**
Computational time for transonic airfoil test case.

| Order | Limiter | Computational time (s) |
|---|---|---|
| 2nd | Venkatakrishnan | 37 |
| 2nd | New | 40 |
| 4th | Venkatakrishnan | 84 |
| 4th | New | 99 |

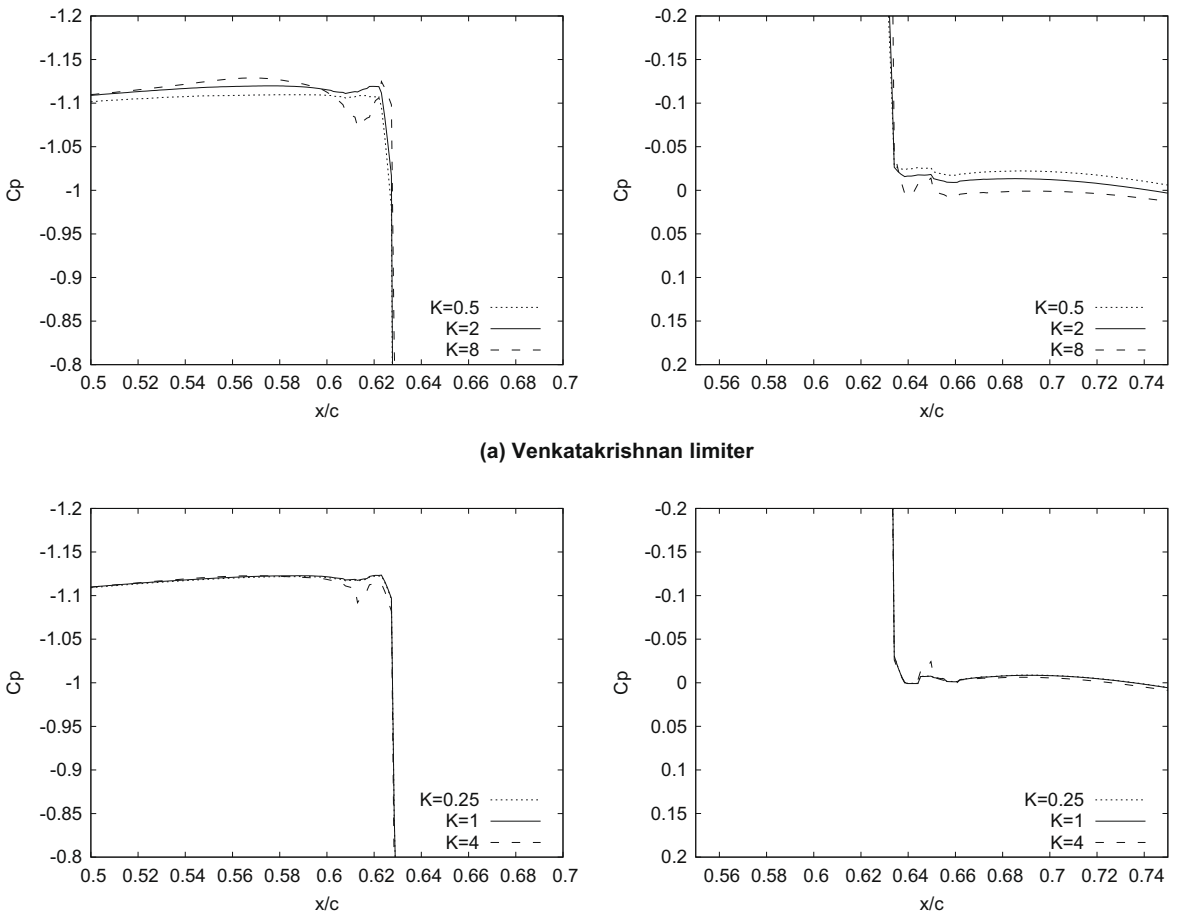


**Fig. 14.** Surface pressure profile close-ups at the upper surface shock for transonic flow over a NACA0012 airfoil using fourth-order scheme.

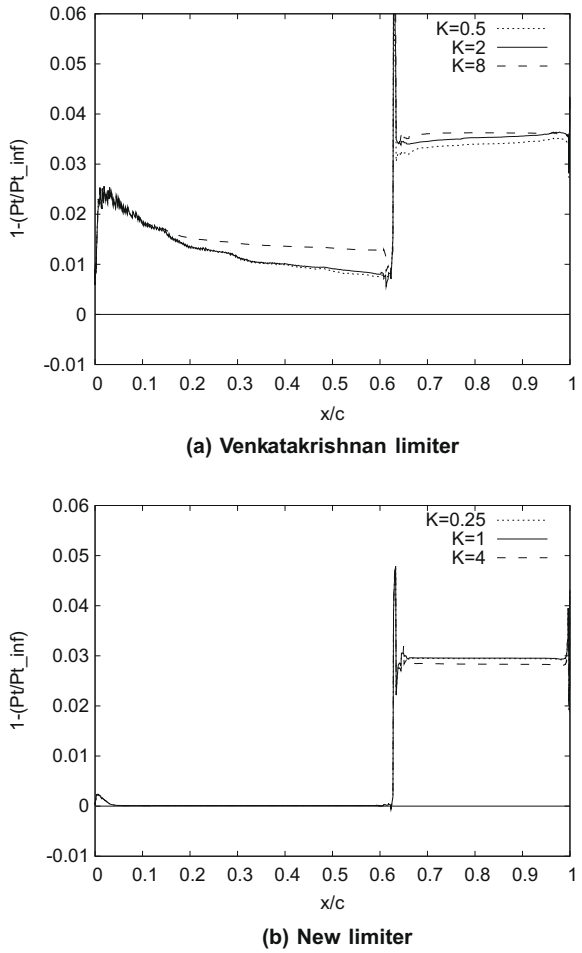


**Fig. 15.** Sensitivity of total pressure along the upper surface of the NACA 0012 airfoil to the choice of limiter tuning parameter.

pressure on the upper surface of the airfoil just upstream of the shock using the fourth-order scheme. The solution using Venkatakrishnan's limiter exhibits a strong sensitivity to the value of the parameter. Specifically, $K = 0.5$ results in a lower peak pressure ahead of the shock, while $K = 8$ results in significant oscillations. The result using the new limiter shows less sensitivity. Specifically, the results using $K = 0.25$ are virtually indistinguishable from those with $K = 1$ while the results with $K = 4$ result in some oscillation.

To further examine the effect of this parameter on the dissipation of the scheme, the stagnation pressure along the upper surface of the airfoil is shown in Fig. 15. For Venkatakrishnan's scheme the value of the tuning parameter has little effect on the total pressure loss near the leading edge of airfoil. However, the stagnation pressure loss across the shock exhibits a strong dependence on this parameter. The new limiter exhibits almost no sensitivity to the parameter ahead of the shock. Downstream of the shock the results using parameters $K = 0.25$ and $K = 1$ are indistinguishable while the stagnation pressure with $K = 4$ is higher.

## 6. Conclusion

A new unstructured grid limiter broadly based on the framework introduced by the Barth and Jespersen limiter has been developed specifically for high-order schemes. Like the Venkatakrishnan limiter, it is designed to be differentiable to enable good convergence to steady state by implicit schemes. To achieve this and to maintain high-order accuracy, a new function defining the relation between the limiter value and the unlimited reconstruction at Gauss points has been constructed. To preserve accuracy at smooth extrema, a smooth switch disables the limiter in regions of nearly uniform flow. To avoid limiting regions of smooth flow near boundaries, the range defining monotonicity is carefully expanded based on a constant momentum extrapolation of conditions beyond the boundary. Application of the limiter is avoided at stagnation points by smoothly disabling it in regions of low Mach number.

The results indicate that the new limiter is effective in maintaining high-order accuracy in smooth flows while effectively suppressing oscillations near shocks. Additionally, the new scheme is also relatively insensitive to tuning parameters which should lead to robustness and reproducibility of solutions. Although the greatest gains in accuracy are seen when using a high-order scheme, the new limiter is also effective in reducing the dissipation and increasing the accuracy of second-order schemes relative to the currently most widely used limiter. Since only minor modifications to the reconstruction procedure are needed, the addition of the new method to existing solvers should be relatively straightforward.

Our approach could be improved in at least two ways. First, we would strongly prefer to eliminate all limiter activity when the solution is smooth, regardless of local mesh regularity. One possible solution to this problem is to use the residual from the least-squares problem as a smoothness measure, turning off the limiter on this basis much as we currently do when the solution is flat; such a fix might well subsume our current approach to flat regions and wall effects. Second, there may be situations in which elimination of the highest order terms would enforce monotonicity without requiring changes to other terms. This would be desirable from the point of view of accuracy, although we have not investigated whether such situations are common or exceedingly rare.

Although the present work presents only inviscid results in two dimensions, the extension to viscous flows and three dimensions should be relatively simple. Specifically, for viscous flows the stagnation region fix should be sufficient in eliminating the effect of the limiter near walls making the wall ghost value fix unnecessary. For three-dimensional inviscid flows the wall ghost value fix will need to account for streamline curvature even though streamlines will not be coordinate aligned.

## References


[1] D. Zingg, S. De Rango, M. Nemec, T. Pulliam, Comparison of several spatial discretizations for the Navier–Stokes equations, Journal of Computational Physics 160 (2000) 683–704.
[2] S. De Rango, D.W. Zingg, Higher-order spatial discretization for turbulent aerodynamic computations, American Institute of Aeronautics and Astronautics Journal 39 (7) (2001) 1296–1304.
[3] T.J. Barth, P.O. Frederickson, Higher order solution of the Euler equations on unstructured grids using quadratic reconstruction, AIAA paper 90-0013, January 1990.
[4] T.J. Barth, Aspects of unstructured grids and finite-volume solvers for the Euler and Navier–Stokes equations, in: Lecture Series 1994-05, von Karman Institute for Fluid Dynamics, Rhode-Saint-Genèse, Belgium, 1994.
[5] M. Delanaye, J.A. Essers, Quadratic-reconstruction finite volume scheme for compressible flows on unstructured adaptive grids, American Institute of Aeronautics and Astronautics Journal 35 (4) (1997) 631–639.
[6] B. van Leer, Towards the ultimate conservative difference scheme. V. A second-order sequel to Godunov's method, Journal of Computational Physics 32 (1979) 101–136.
[7] T.J. Barth, D.C. Jespersen, The design and application of upwind schemes on unstructured meshes, AIAA paper 89-0366, January 1989.
[8] V. Venkatakrishnan, On the accuracy of limiters and convergence to steady-state solutions, AIAA paper 93-0880, January 1993.
[9] T.J. Barth, Recent developments in high order *k*-exact reconstruction on unstructured meshes, AIAA paper 93-0668 January 1993.
[10] C.F. Ollivier-Gooch, High-order ENO schemes for unstructured meshes based on least-squares reconstruction, AIAA paper 97-0540, January 1997.
[11] P. Geuzaine, M. Delanaye, J.-A. Essers, Computation of high Reynolds number flows with an implicit quadratic reconstruction scheme on unstructured grids, in: Proceedings of the 13th AIAA Computational Fluid Dynamics Conference, American Institute of Aeronautics and Astronautics, 1997, pp. 610–619.
[12] A. Nejat, C. Ollivier-Gooch, A high-order accurate unstructured finite volume Newton–Krylov algorithm for inviscid compressible flows, Journal of Computational Physics 227 (4) (2008) 2592–2609, doi:10.1016/j.jcp.2007.11.011.
[13] R. Abgrall, On essentially non-oscillatory schemes on unstructured meshes: analysis and implementation, Journal of Computational Physics 114 (1) (1994) 45–58.
[14] C.-W. Shu, T.A. Zang, G. Erlebacher, D. Whitaker, S. Osher, High-order ENO schemes applied to two- and three-dimensional compressible flow, Applied Numerical Mathematics 9 (1) (1992) 45–71.
[15] A.G. Godfrey, C.R. Mitchell, R.W. Walters, Practical aspects of spatially high-order accurate methods, American Institute of Aeronautics and Astronautics Journal 31 (9) (1993) 1634–1642.
[16] O. Friedrich, Weighted essentially non-oscillatory schemes for the interpolation of mean values on unstructured grids, Journal of Computational Physics 144 (1) (1998) 194–212.
[17] C.Q. Hu, C.W. Shu, Weighted essentially non-oscillatory schemes on triangular meshes, Journal of Computational Physics 150 (1) (1999) 97–127.
[18] G.-S. Jiang, C.-W. Shu, Efficient implementation of weighted ENO schemes, Journal of Computational Physics 126 (1) (1996) 202–228.
[19] C.F. Ollivier-Gooch, Quasi-ENO schemes for unstructured meshes based on unlimited data-dependent least-squares reconstruction, Journal of Computational Physics 133 (1) (1997) 6–17.
[20] C.F. Ollivier-Gooch, M. Van Altena, A high-order accurate unstructured mesh finite-volume scheme for the advection–diffusion equation, Journal of Computational Physics 181 (2) (2002) 729–752.
[21] C. Michalak, C. Ollivier-Gooch, Matrix-explicit GMRES for a higher-order accurate inviscid compressible flow solver, in: Proceedings of the 18th AIAA Computational Fluid Dynamics Conference, 2007.
[22] P.K. Sweby, High resolution schemes using flux limiters for hyperbolic conservation laws, SIAM Journal on Numerical Analysis 21 (5) (1984) 995–1011, doi: http://dx.doi.org/10.1137/0721062.
[23] G.D. van Albada, B. van Leer, W.W. Roberts Jr., A comparative study of computational methods in cosmic gas dynamics, Astronomy and Astrophysics 108 (1982) 76–84.
[24] Y. Saad, M.H. Schultz, GMRES: a generalized minimal residual algorithm for solving nonsymmetric linear systems, SIAM Journal of Scientific and Statistical Computing 7 (3) (1986) 856–869.